The Simulated Binding of (±)-2,3-Dihydro-5,6-dimethoxy-2-[[1-(phenylmethyl)-4-piperidinyl]methyl]-1*H*-inden-1-one Hydrochloride (E2020) and Related Inhibitors to Free and Acylated Acetylcholinesterases and Corresponding Structure−Activity Analyses

Atsushi Inoue, Takatoshi Kawai, Misako Wakita, Youichi Iimura, Hachiro Sugimoto, and Yoshiyuki Kawakami*

Tsukuba Research Laboratories, Eisai Co., Ltd., 1-3, Tokodai 5-chome, Tsukuba-shi, Ibaraki 300-26, Japan

The simulated binding profiles of acetylcholine, ACh, and the inhibitor (±)-2,3-dihydro-5,6-dimethoxy-2-[[1-(phenylmethyl)-4-piperidinyl]methyl]-1*H*-inden-1-one hydrochloride (E2020), **1**, and some of its analogs to acetylcholinesterase, AChE, were determined using full force field energetics and allowing complete conformational flexibility in both the ligand and receptor. A new mode of binding of ACh to AChE was found which involves the carboxyl oxygen of ACh interacting with Gly 118 and 119. Multiple modes of binding of **1** and some of its analogs were found which include alignment models observed in previous more restricted modeling studies. The key ligand−receptor interactions identified, and the corresponding energetics, are consistent on a relative basis, with observed binding constants for both the individual isomers of each of the inhibitors, as well as among the inhibitors themselves. The multiple modes of binding of **1** to AChE arises from small changes in binding at a single subsite and also from multiple subsite changes. Thus, an independent subsite model for ligand−receptor binding holds for some modes of binding, but not for others. A comparison of the simulated AChE−**1** (and analog inhibitors) binding models to the receptor-independent 3D-QSARs previously developed for this class of inhibitors reveals extensive mutual consistency. The findings from these two modeling studies provides greater guidelines for inhibitor design than can be realized from either one. The combined docking and 3D-QSAR studies permit a detailed understanding of the SAR of more than 100 compound **1** analog inhibitors. A simple molecular recognition model can also be gleaned from the docking studies. A cylindrical "plug" (the inhibitor) having a large dipole moment must sterically fit into a cylindrical hole (the active site gorge of AChE), the lining of which also has a large dipole moment. Our simulations suggest that the dynamic "back door" to the active site of AChE does not form a large enough opening for sufficiently long time periods so as to be an effective entrance/exit pathway.

Introduction

Clinical studies with the reversible acetylcholinesterase (AChE) inhibitor, (±)-2,3-dihydro-5,6-dimethoxy-2-[[1-(phenylmethyl)-4-piperidinyl]methyl]-1*H*-inden-1-one hydrochloride (E2020),[1] **1**, see Figure 1, have suggested that it may be effective for treatment of Alzheimer's disease where the cholinergic function is selectively, and irreversibly, affected in this senile dementia disease.[2] This optimistic outlook now appears to be justified as **1** has successfully completed phase III clinical studies in the United States for treatment of senile dementia disease. The mechanism proposed to explain the memory improvement through AChE inhibition is an increase in acetylcholine (ACh) levels in the central cholinergic synapses involved in the memory circuit.[3−6] THA (tetrahydroaminoacridine, Figure 1) recently became the first available agent for the treatment of Alzheimer's disease in the United States. However, the aminoacridines, in general, suffer from dose-limiting hepatotoxicity which is believed to be structure related.[7] Compound **1** appears to be devoid of such an unfavorable side-effect profile probably because of its novel benzylpiperidine structure. Moreover, **1** is the first compound of a new class of AChE inhibitors having an *N*-benzylpiperidine and an in-

danone moiety which is selective. Compound **1** shows greater selectivity for AChE than for butyrylcholinesterase and is expected not to have any significant peripheral effect.[8] The enantiomers of **1** exhibit near identical pharmacological profiles, including inhibitory effects, and consequently, **1** is being developed as a racemic mixture.

A number of compounds have been made and tested by Eisai in the quest for a potent and selective AChE inhibitor which has been achieved with **1**. The corresponding structure−activity relationship (SAR) data has been used in computer-assisted molecular design (CAMD) studies[9−12] to develop guidelines for target synthesis and, retrospectively, to explain unusual SAR behavior. Some groups have also undertaken the design and synthesis of compounds similar to **1** which incorporate bioisosteric replacements for the indanone ring.[13,14] Very recently, a 3D-QSAR using comparative molecular field analysis, CoMFA, has been reported for a set of AChE benzylpiperidine inhibitors.[15] All of the CAMD studies have been receptor-independent in that the geometry of AChE had not been determined and was available for structure-based design studies. Sussman et al., however, have reported the crystal structure of AChE from *Torpedo californica* electric organ.[16] The availability of the geometry of an AChE presents the opportunity to extend the CAMD studies to ligand−receptor docking analyses and to support, refute, and/
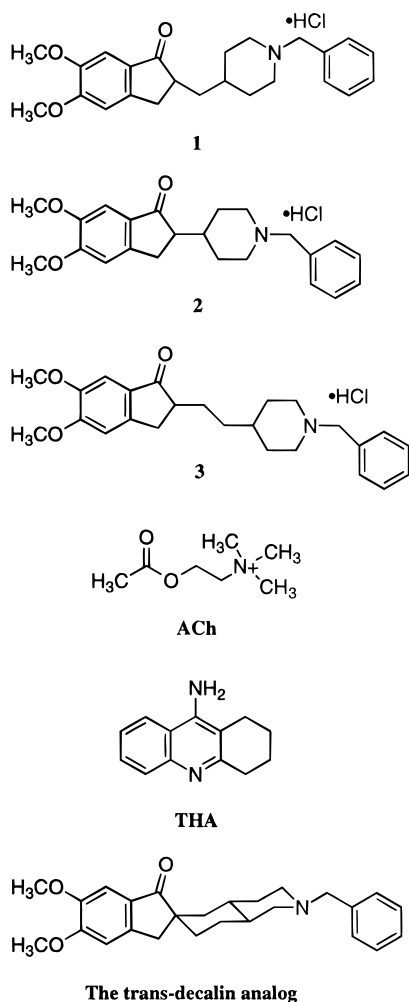
Figure 1. The chemical structures of **1**, **2**, **3**, ACh, THA, and the *trans* decalin analog.

or refine previous CAMD studies. The crystal structure of AChE has, in fact, already been used in nonenergetic docking studies of **1** and some indanone isosteric analogs of **1** and in the prediction of a compound **1** binding site on AChE.[17,18]

The goals of the ligand−receptor binding studies reported here as follows: (1) to compare/contrast and reconsile the 3D-QSARs (receptor-independent) developed for some **1** analogs and the preferred binding geometries and energetics found in the binding analyses, (2) to compare the predicted (receptor-independent) "active" conformations and molecular shapes of some **1** analogs to those realized in these binding studies, (3) to compare and contrast the preferred ligand−receptor binding geometries found in these studies to those proposed in the other docking studies, and (4) to explain/ rationalize some of the SAR observed for certain **1** analogs in terms of multiple AChE binding sites; (5) as shown in Tables 1 and 2, **1** and related compounds, **2** (1-benzyl-4-(5,6-dimethoxy-1-oxoindan-2-yl)piperidine hydrochloride) and **3** (1-benzyl-4-[(5,6-dimethoxy-1-oxoindan-2-yl)ethyl]piperidine hydrochloride), see Figure 1, seem to bind to both the free enzyme and the acylated enzyme to block both Michaelis complex formation and the deacetylation processes.[19] There does not appear to be any CAMD docking studies done to provide a basis for this dual inhibitory binding. Hence, both the free enzyme (E) and a model acylated enzyme (EA) have been considered in the binding studies reported here

with the objective of identifying binding modes which could yield dual inhibition.

Methods

1. Receptor AChE Models. The atomic coordinates of AChE were obtained from the crystal structure of AChE isolated from *T. californica*, as deposited in the Brookhaven Protein Data Bank (PDB entry: 1ACE). Hydrogen atoms were added by the program PDBFIL[20] after deleting the crystalline water molecules present in the X-ray structure, and aliphatic carbon−hydrogen groups were treated as united atoms.

The three-dimensional structure of the acylated enzyme has not been determined. The EA model used in this study was generated from the X-ray structure of AChE as follows: (A) A covalent bond was constructed between the carbon atom of the carbonyl group in acetate and the oxygen in the side chain of Ser 200. (B) The local geometry of the modified enzyme was constructed with distance constraints between the oxygen atom of the carbonyl group in the acylated Ser 200 residue and the three nitrogen atoms in the backbones of Gly 118, Gly 119, and Ala 201 that form the "oxyanion hole". This hole is the specific binding site for the carbonyl oxygen of ACh. (C) Calculations were then carried out for this trial geometry using AMBER [3.0 rev A] minimizing the energy without the distance constraints.[21] After 100 cycles of minimization of the EA, two of three hydrogen bonds involving the Ser 200 carbonyl oxygen were preserved. The distance between the C=O of acylated Ser 200 and the N−H of Ala 201 was 3.3 Å, indicating that these groups do not hydrogen bond.

2. Ligand Models. The atomic coordinates of **1** were taken from its crystal structure, and the other two analogs were modeled from **1**.[10,11] The geometries of six structures, including both the *R* form and *S* form of each inhibitor, were optimized by the MNDO method of the MOPAC program.[22] The atomic charges, electrostatic potentials, and dipole moments were calculated using these optimized structures. The electrostatic potential of AChE was generated using the program package, "Insight/Delphi".[23]

3. Ligand−Receptor Docking. Four hierarchical operations were sequentially applied in the ligand−receptor binding analysis of each AChE inhibitor. The four operations are listed in Figure 2 and are discussed below. In composite, they constitute a comprehensive approach to identifying plausible ligand receptor binding sites.

Operation 1: Mapping the Receptor Site by Grid-Point Searching. Grid-point probe energy data were calculated on 46970 grid-points within a box of dimensions 18.0Å×20.8Å× 19.6Å for the E, and on 46 416 grid points for the EA using the scheme in program GREEN.[20] The dimensions and location of the box were defined to include the entire AChE active-site gorge which incorporates the active-site gorge of both the E and EA enzyme models. The grid-point data provides information on the physical and chemical environment of the gorge. In this study the van der Waals potential of five probe atoms (C, H, N, O, S), the electrostatic potential, and hydrogen-bonding characteristics were used to generate grid-point data. Hydrogen-bonding characteristics are defined in terms of the bonding of an atom when it makes a hydrogen bond with another heteroatom. Character is one of four types: donor, acceptor, both, or none. The electrostatic interaction energy was calculated using a Coulomb function with a molecular dielectric of 4.0. The grid spacing was set to 0.4 Å.

The grids shown in Figure 3 represent the shapes of the cavities of (A) E and (B) EA. The grid color is classified according to electrostatic potential. Blue regions indicate negative charge sites of the enzyme. The darkest blue region arises from Glu 199 (bottom of the cavity), and the next two most negative charge sites are from Asp 72 and Tyr 334 (middle, right) in both enzyme models. No positive charge site as intense as the negative site of Glu 199 is observed. There are two Trp residues at the bottom entrance to the cavity which form planar walls and prefer to interact with hydro-

Table 1. Intramolecular, ΔE_{intra}, Intermolecular, ΔE_{inter}, and Total Binding Energy, ΔE_{total}, for ACh, **1**, **2**, and **3** Binding to AChE[a]

Part A: Binding Models Proposed and Calculated for ACh−E Complexes

	energies			key binding interactions for ACh−AChE	
model no.	ΔE_{intra} (kcal/mol)	ΔE_{inter} (kcal/mol)	ΔE_{total} (kcal/mol)	KBI 1	KBI 2
proposed	0.6	−24.6	−24.0	Trp 84	
1	0.5	−27.9	−27.2	Gly 118	Gly 119

Part B: **1** [K_i = 3.35 nM (R), 17.5 nM (S) K_i* = 6.73 nM (R), 37.6 nM (S)]

model no.	ΔE_{intra} (kcal/mol)	E_{inter} (kcal/mol)	E_{total} (kcal/mol)	KBI 1[b]	KBI2[c]	KBI 3[d]	KBI 4[e]	KBI 5[f]
1(R)	0.6	−46.1	−45.5	W279/3.47	R289/3.50[g]	Y121/2.89	D72/3.32	W84/3.81
2(R)	0.2	−51.3	−51.1	perpend[h]		F327/2.96[g]	F330/4.97[i]	W84/3.52
3(R)	0.0	−43.6	−43.6	W279/3.97	R289/2.94[g]	Y70/3.50	D72/2.93	W84/4.16
4(R)	2.0	−44.1	−42.1	W279/3.90			D72/3.00	W84/3.53
5(R)	0.7	−45.3	−44.6	W279/3.69	R289.3.38[g]	Y121/3.18	D72/3.30	W84/3.83
6(S)	4.5	−46.9	−42.4	W279/4.89	R289/3.03[g]	Y121/3.22		W84/3.85
7(S)	3.4	−45.3	−41.9	perpend[h]		Y121/3.78		W84/3.85
8(S)	6.8	−44.3	−37.5	W84/3.58	Y130/3.39	Y121/2.94		
9(S)	5.1	−32.7	−27.6			Y70/3.56		
10(S)	1.8	−45.2	−43.4	W279/4.50	R289/3.64[g]	Y70/3.56	D72/3.69	W84/3.52
11(S)	5.8	−48.5	−42.7		F288/2.98[g]	Y121/2.79	D72/3.57	

Part C: **2** [K_i = 122.00 nM, K_i* = 54.00 nM]

model no.	ΔE_{intra} (kcal/mol)	E_{inter} (kcal/mol)	E_{total} (kcal/mol)	KBI 1	KBI 2	KBI 3	KBI 4	KBI 5
1(R)	3.0	−42.8	−39.8	perpend[h]		F330/3.36		W84/3.48
2(R)	1.4	−44.9	−43.5		Y334/2.76[g]			W84/3.53
3(R)	4.2	−46.1	−41.9			Y121/2.79		perpend[h]
4(R)	4.6	−46.6	−42.0			D72/3.29		W84/3.58
5(R)	4.1	−44.1	−40.0		Y334/3.41	D72/3.29		
6(R)	4.9	−42.7	−37.8		G335/3.22		Y121/2.79	
7(S)	2.9	−42.4	−39.5		G335/3.30[g]		Y121/3.01	W84/3.41
8(S)	2.9	−43.7	−40.8				Y121/3.63	W84/4.21
9(S)	1.5	−43.8	−42.3	perpend[h]			Y121/3.16	
10(S)	1.6	−38.3	−36.7			Y121/3.04	D72/2.83	
11(S)	1.2	−42.8	−41.6	perpend[h]	G335/3.07[g]			W84/3.37
12(S)	0.0	−41.7	−41.7				Y121/2.79	
13(S)	0.3	−44.7	−44.7	perpend[h]		Y121/2.58		W84/3.38

Part D: **3** [K_i = 18.70 nM, K_i* = 47.00 nM]

model no.	ΔE_{intra} (kcal/mol)	E_{inter} (kcal/mol)	E_{total} (kcal/mol)	KBI 1	KBI 2	KBI 3	KBI 4	KBI 5
1(R)	0.8	−52.6	−51.8		S286/3.10[g]	Y121/3.57		
2(R)	0.1	−53.0	−52.9			F288/2.92	Y121/3.27	W84/3.28
3(R)	2.3	−51.0	−48.7		G335/3.13[g]	F288/2.89	D72/3.28	W84/3.23
4(R)	0.7	−47.2	−46.5	W279/3.20		Y70/2.73		W84/3.74
5(R)	0.0	−50.7	−50.7			Y121/3.45	F330/4.38[i]	W84/3.37
6(R)	2.1	−51.3	−49.2			F288/2.91	D72/3.29	W84/3.40
7(S)	1.8	−47.0	−45.2	W279/4.03		Y70/2.88	Y121/3.94	W84/3.55
8(S)	6.5	−48.1	−41.6		G335/31[g]	F288/2.84		W84/3.75
9(S)	3.7	−52.0	−48.3	W279/3.75		Y121/3.59	F330/4.65[i]	W84/3.71
10(S)	4.0	−50.7	−46.7	W279/3.84		Y70/3.43	F330/4.53[i]	W84/3.50
11(S)	2.7	−48.4	−45.7	W279/3.98		Y70/2.81		W84/3.37
12(S)	6.1	−48.8	−42.7	perpend[h]			D72/3.12	

[a] The KBIs are also given and their definitions are presented in the text and in the following footnotes. The K_is are the observed binding constants to E for each of the isomers, and the K_i*s are the observed binding constants to EA. [b] Trp 279 whose indole side chain is parallel to the indanone ring and the average distance between indanone ring and indole ring of the residue. [c] Type and number of the residue interacting with the methoxy group and the average distance between the two heteroatoms. [d] Interaction (and average distance) with the carbonyl group of the indanone ring. [e] Interaction (and average distance) with the protonated NH group of the piperidine ring. [f] Same as b, but for Trp 84. [g] This interaction distance can accommodate a water bridge. [h] The indanone ring is perpendicular to the indole side chain in Trp 279. [i] The NH points toward the center of the phenyl ring side chain of Phe 330.

phobic groups such as other aromatic rings. The middle of the cavity is the most narrow part of the active-site gorge due to Tyr 121.

The shape of the cavity of the EA is slightly different from that of E in the near vicinity of the modified residue. The Ser 200 carbonyl group is directed toward the "oxyanion hole" and the methyl group toward the cavity so that inhibitors of E can still interact with the EA at the active site. The electrostatic character of the contact surface of the modified side chain in the EA model is neutral.

Operation 2: Construction of the Set of Possible Intermolecular Binding Sites ("Hooks"). Plausible initial binding-site coordinate sets were generated on the basis of possible hydrogen bonding between donor−acceptor hetero-
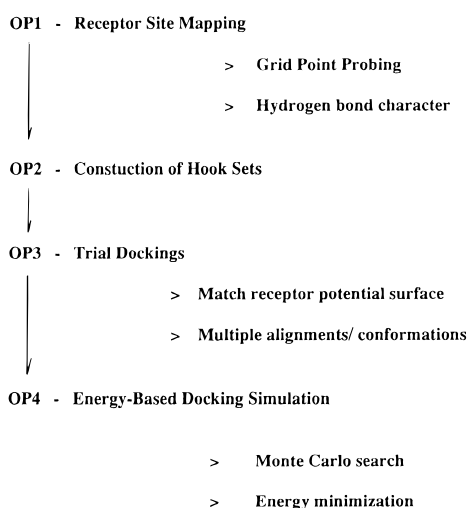
atom pairs of an inhibitor and the active-site gorge of the AChE receptor. The program CAVHET[24] was used to generate dummy heteroatoms of a hypothetical inhibitor for each of the grid points in the cavity and then to search the enzyme heteroatom hooks for those in which (1) the distance between the dummy heteroatoms and the enzyme heteroatom hook was within 4 Å and (2) the angle of the acceptor−H-donor was within 60° of being linear.

Operation 3: Generation of Trial Docking Alignments and Ligand Conformation. Initial docking alignments were generated by matching the grid shape and contact potential surface of the enzyme cavity to that of the electrostatic potential surface of the inhibitor using rigid, manual fitting. Each of the complementary charge and steric surface matching

Table 2. The Same Information as Given in Table 1, but for **1**, **2**, and **3** Binding to the EA Model

model no.	ΔE_{intra} (kcal/mol)	E_{inter} (kcal/mol)	E_{total} (kcal/mol)	KBI 1[a]	KBI 2[b]	KBI 3[c]	KBI 4[d]	KBI 5[e]	rms[i] (Å)
			Part A: **1** [K_i^* = 9.48 nM]						
1(R)	0.6	−46.2	−45.6	W279/3.51	R289/3.50[f]	Y121/2.83	D72/3.46	W84/4.13	±0.13
2(R)	0.8	−51.6	−50.8	perpend[g]	S286/3.49[f]		F330/4.91[h]	W84/3.62	0.11
3(R)	0.0	−45.0	−45.0	W279/3.99	R287/2.97[f]	Y70/3.37	D72/3.11	W84/4.35	0.11
4(R)	2.1	−44.1	−42.0	W279/3.91			D72/3.01	W84/3.52	0.03
5(R)	1.6	−51.7	−50.1		S286/3.40[f]	Y121/2.82	F330/3.60[h]	W84/3.69	1.86
6(S)	3.7	−48.8	−45.1	W279/4.90	S286/4.40[f]			W84/4.46	0.32
7(S)	3.1	−53.3	−50.2	perpend[g]	S286/2.79[f]	Y121/3.35		W84/3.49	0.75
8(S)	2.2	−46.8	−44.6		S81/3.38				2.35
9(S)	5.9	−33.7	−27.8	W279/3.65		D72/2.65		W84/4.02	0.14
10(S)	0.1	−46.7	−46.6	W279/4.02	R289/2.99[f]	Y70/3.23	D72/3.90	W84/3.94	0.20
11(S)	6.2	−48.8	−42.6		S286/3.02[f]	Y121/2.83			0.08
			Part B: **2** [K_i^* = 54.0 nM]						
1(R)	5.0	−45.4	−40.4	perpend[g]		F330/3.09[f]		W84/3.44	±0.74
2(R)	3.0	−45.7	−42.7		Y334/2.70			W84/3.38	0.12
3(R)	2.9	−47.7	−44.8		Y70/3.04[f]				0.16
4(R)	5.0	−49.0	−44.0						0.16
5(R)	3.3	−46.2	−42.9		Y70/3.22	Y121/3.94			0.16
6(R)	2.4	−43.7	−41.3			F288/3.94	Y121/3.42		0.81
7(R)	5.0	−42.7	−37.7		G335/3.23[f]		Y121/2.99	W84/3.33	0.07
8(S)	2.5	−43.5	−41.0		R289/3.52[f]		Y121/3.21	W84/4.23	0.29
9(S)	2.1	−44.7	−42.6		S286/3.16[f]		Y121/3.02		0.61
10(S)	0.0	−39.9	−39.9				Y334/3.92[h]		0.95
11(S)	2.7	−43.4	−40.7		G335/2.98[f]		Y121/2.86		0.16
12(S)	1.4	−41.6	−40.2	perpend[g]	Y70/4.20[f]		Y121/2.77		0.04
13(S)	1.1	−44.8	−43.7	perpend[g]	S286/3.16[f]		Y121/3.18		1.87
			Part C: **3** [K_i^* = 27.0 nM]						
1(R)	1.9	−52.7	−52.8	perpend[g]	S286/3.06[f]				±0.06
2(R)	1.5	−53.1	−51.6	W279/3.54	G335/3.20	F288/2.94	Y121/3.23	W84/3.25	0.05
3(R)	2.4	−50.7	−48.3	W279/3.55	G335/3.09[f]	F288/2.90	D72/3.33	W84/3.38	0.13
4(R)	1.4	−48.0	−46.6	W279/4.30		Y70/2.83		W84/3.78	0.16
5(R)	0.0	−54.6	−54.6	W279/4.25	R289/2.93[f]		F330/4.89[h]	W84/3.40	0.26
6(R)	1.3	−51.6	−50.3	W279/3.62	G335/3.04[f]	F288/3.02	Y334/3.78[h]	W84/3.86	0.42
7(S)	5.1	−52.1	−47.0	W279/3.90		Y70/3.91		W84/3.41	0.61
8(S)	3.7	−48.0	−44.3		G335/3.27[f]	F288/2.97		W84/3.77	0.12
9(S)	4.9	−54.4	−49.5		R289/4.23[f]	Y121/3.17	F330/4.81[h]		0.67
10(S)	2.1	−52.0	−49.9	W279/4.02	W279/4.91[f]		F330/4.47[h]	W84/3.61	0.45
11(S)	5.5	−52.3	−46.8	W279/3.94		Y70/4.27		W84/3.41	0.73
12(S)	8.1	−50.0	−41.9	perpend[g]	S283/3.84	R289/3.19	D72/3.11		0.34

[a–h] See footnotes $b-i$ in Table 1. [i] Average root-mean-square difference in the ligand atomic coordinates for EA compared to E.

OP1 - Receptor Site Mapping

> Grid Point Probing

> Hydrogen bond character

OP2 - Constuction of Hook Sets

OP3 - Trial Dockings

> Match receptor potential surface

> Multiple alignments/ conformations

OP4 - Energy-Based Docking Simulation

> Monte Carlo search

> Energy minimization

Figure 2. The search and alignment operations used in the docking simulations.

alignments, for a given enzyme−inhibitor complex, were then refined using GREEN[20] in the following manner: (1) An intermolecular hydrogen bond was generated between each of the extracted enzyme heteroatom hooks and a heteroatom in the inhibitor, i.e., oxygen atoms of the methoxy and carbonyl groups of the indanone ring and the nitrogen atom of the piperidine moiety. (2) An inhibitor was refit into the binding site, subject to retaining the intermolecular hydrogen bonds, by perturbation rotations of both ligand and AChE torsion angles to eliminate bad-contact atom-pair interactions. Bad-contact interactions were monitored by the intermolecular energy using the 3D grid-point data. This sequence of operational calculations allows full ligand and receptor flexibility. In contrast, the frozen protein model does not allow exploration of all conformational and ligand−receptor interaction degrees of freedom.

Operation 4: Energy-Based Docking Simulations. Monte Carlo sampling was used to establish intermolecular low-energy alignments, as well as conformations of the inhibitors, for every initial complex model. In this method, the total intermolecular energy, as defined in eq 1, was used as the index

$$E_{ei} = \sum_m (G_{vdw}(m,k_m) + G_{elc}(m,q_m)) \qquad (1)$$

of relative stability. For each atom, m, of the inhibitor, the grid-point VDW energy ($G_{vdw}(m,k_m)$) and the grid-point electrostatic energy (including hydrogen bonding) ($G_{elc}(m,q_m)$) were determined by interpolating from the values of the eight grid points on the vertices of a cube containing atom m. k_m is the atom type in eq 1. Fifty thousand Monte Carlo iterations were performed at 300 K for maximum step widths of 1° for inhibitor rotation, 0.1 Å for inhibitor translation, and 5° in torsion angle rotations. Each of the most stable inhibitor−enzyme geometries found by grid searching were then optimized using the simplex method.[25]

The same procedure described above was repeated using the minimum energy complexes found by eq 1 as starting geometries for the AMBER force field,[21] as expressed by eq 2, to explicitly calculate the intermolecular energy. The first summation term in eq 2 is the Lennard−Jones 6−12 potential. The second term accounts for the electrostatic interactions, and the third term treats the interaction of the hydrogen-bonding atoms.
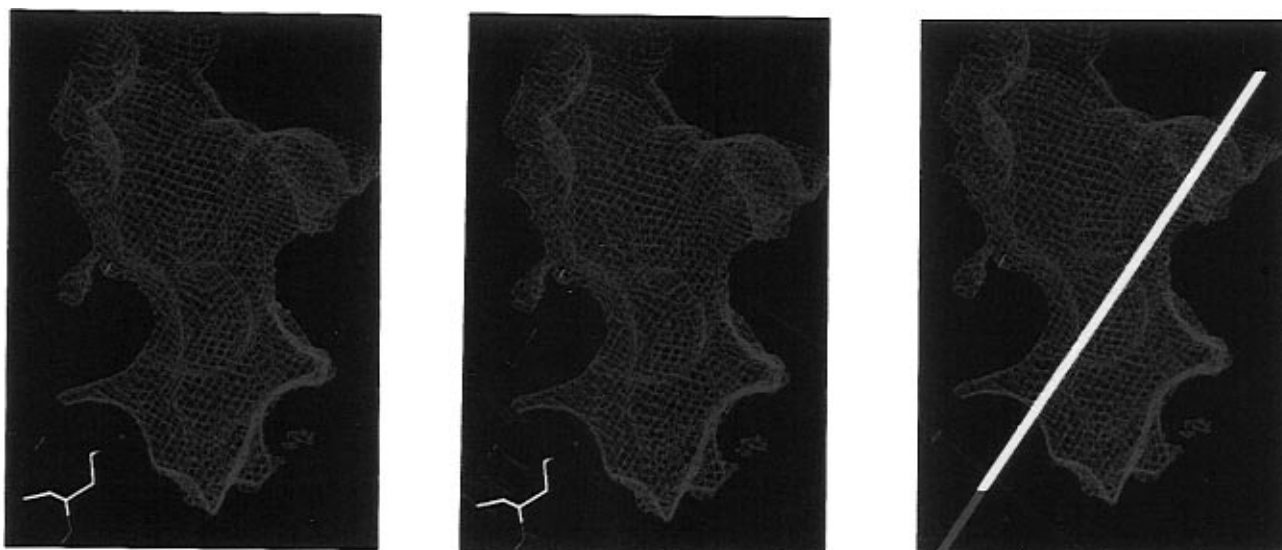
Figure 3. (A, Left) Active-site cavity of E shown in grid surface form. (B, Middle) Active-site cavity of EA shown in grid surface form. (C, Right) The dipole moment of E outlined in the active site cavity.

$$E_{\text{intermolecular}} = \sum_i \sum_j (\text{Ar}_{ij}^{-12} - \text{Br}_{ij}^{-6}) + \sum_i \sum_j q_i q / \text{Er}_{ij} + \\ \sum_i \sum_j (\text{Cr}_{ij}^{-12} - \text{Dr}_{ij}^{-10}) \quad (2)$$

The minimum energy ligand−receptor alignments, that is binding geometries, and corresponding energies, from the AMBER-based simulations were recorded for use in subsequent binding comparison analyses.

Results

1. Binding Models of ACh to AChE. Figure 4 is a side view of the binding region of AChE. The most remarkable feature of this structure is its deep and narrow channel, about 20 Å long and as narrow as 4.5 Å. This gorge penetrates halfway into the enzyme and widens out close to its interior terminus. The active site of AChE lies close to the terminus of this deep and narrow aromatic gorge which is lined with the side chain rings of 14 aromatic amino acid residues. It appears that the size of the active-site pocket is too small for **1**, and its related analogs, to mimic the binding geometry of ACh. It has been suggested[27] that the quaternary group of the choline moiety of ACh makes a close contact with the indole ring of Trp 84. Gly 118 and 119 might be part of an oxyanion hole since these glycines make close contacts to the carboxyl oxygen of ACh in the most stable AChE−ACh complex models. The estimated binding energies, based on the AMBER force field, are given in part A of Table 1, for the overall most stable calculated ACh−AChE complex and for the most stable binding model in which the quaternary group of ACh makes close contact to Trp 84.

2. Dipole Moments of ACh and Inhibitors. Ripoll *et al.*[28] have reported that AChE has a remarkably large dipole moment which is aligned directly along the axis defining the center of the aromatic gorge; see Figure 3C. Dipole−dipole interactions may play an important role in the long-range molecular recognition of AChE ligands. Molecules with complementing dipoles to AChE can be drawn toward, and down, the aromatic gorge, leading to the active site in an orientation in which a matching dipole−dipole interaction is formed. Thus, inhibitors that interact with the enzyme in this orientation are expected to have potent activities, and
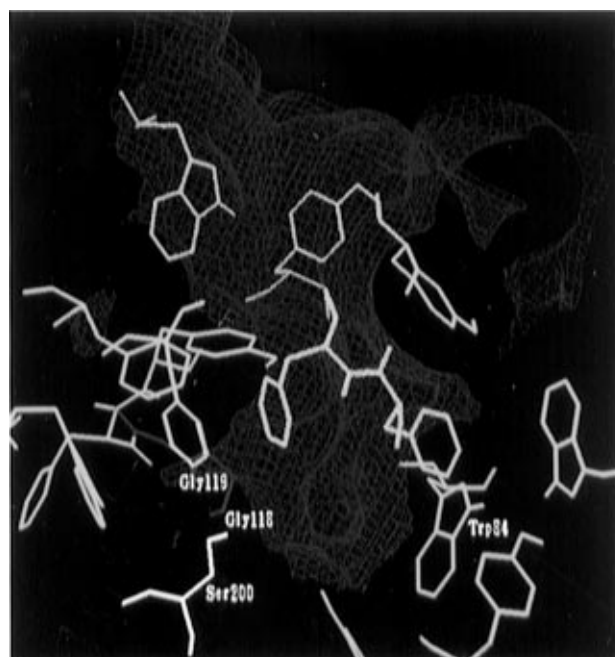

Figure 4. A side view of the active-site gorge of AChE.

some groups have proposed models for the binding of large dipole inhibitors to AChE.[29]

The calculated dipole of ACh, in its bound conformation, is about 23 Debye, while the extended conformation dipole moments of **1**, **2**, and **3** are on the order of 35−50 Debye. The direction of the dipole in each inhibitor runs through the molecule from the benzylpiperidine moiety to the methoxy groups on the indadone ring; see Figure 5. Thus, the calculated large dipoles of ACh and the three inhibitors support the dipole−dipole recognition model mentioned above.[28,29] In essence, one has a tube (the active-site gorge) which possesses a positive charge on one end and a negative charge on the other. A successful inhibitor has a cylindrical shape which can fit into and slide along the inner surface of the tube. The cylindrical (inhibitor) possesses positive and negative charges on its ends so that the preferred orientation and position of the cylinder in the tube is dictated by electrostatic interactions.

3. Binding Models of 1. Five types of key binding interactions, KBI 1−KBI 5, were identified in the
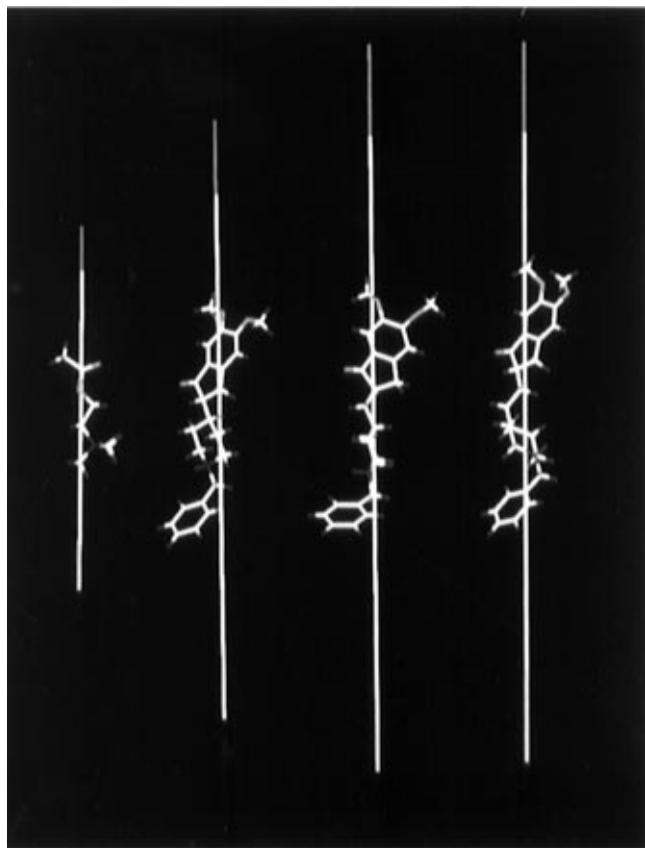
Figure 5. Dipole moments of ACh, **1**, **2**, and **3** superimposed on their respective active conformations.

binding models based on the interactions among AChE and five substructures of **1**. The definitions of the five KBIs are given below and shown in the drawing in Figure 6.

KBI 1: the interaction between the indanone ring and the indole side chain of Trp 279.

KBI 2: the interaction between the methoxy group in the indanone ring and the main-chain carbonyl of Arg 289.

KBI 3: the interaction between the carbonyl group in the indanone ring and the hydroxy group of (a) Tyr 121 or (b) Tyr 70.

KBI 4: the interaction between the NH group in the protonated piperidine and the carboxyl group of (a) Asp 72, (b) the phenyl ring of Phe 330, or (c) the hydroxy group of Tyr 121.

KBI 5: the interaction between the phenyl ring of the benzyl piperidine and the indole ring of Trp 84.

Eleven stable docking models of **1** and E were identified in the docking analysis and are reported in part B of Table 1. The format in Table 1, parts B–D, is to list each of the stable docking models, their respective intramolecular ligand energies, the intermolecular energies, the "total" binding energies, and the "extent" of realizing each of the KBIs for each binding mode. In general, all of the docking models have the benzyl group at the bottom of the active-site cavity and the indanone ring located at the entrance to the cavity. The piperidine ring lies at the narrowest part of the gorge in the binding cavity. The orientation of the piperidine ring in these binding models (KBI 4) can be partitioned into three classes: (a) the NH in the protonated piperidine points toward the charged carboxylate side chain of Asp 72 in six models, (b) the NH points toward the center of the phenyl ring side chain of Phe 330 in one model,

and (c) the NH points toward the hydroxy side chain of Tyr 121 in three models.

In eight models the benzyl ring is parallel to the indole side chain of Trp 84 (KBI 5). The average distance between the two rings is 3.83 Å.

In five of the 10 models the carbonyl group of **1** forms a hydrogen bond with the hydroxyl group of Tyr 121 at an average distance of 3.17 Å (KBI 3a). In one binding model, for the *S* form of **1**, the carbonyl group of the indanone ring forms a hydrogen bond with the hydroxy group of Tyr 70 at a distance of 3.16 Å (KBI 3b).

In five of the inhibitor–enzyme docking models the average distance between the oxygen in a methoxy group of the indanone ring and the carbonyl oxygen in Arg 289 is 3.29 Å (KBI 2). This interaction distance can accommodate a water bridge.[18] In five of the 10 models the indanone ring is parallel to the indole side chain of Trp 279 which is at the entrance to the cavity (KBI 1). The average distance between the rings is 3.82 Å. In the other models the indanone ring is perpendicular to the indole side chain of Trp 279.

Overall, the **1**–E energy-based docking models suggest the possibility of multiple binding modes for **1** which differ from one another with respect to isomer, the indanone ring, the piperidine ring and the benzyl ring subinteractions with E. The lowest total energy **1***R* (model 2) and **1***S* (model 10) binding modes to E are shown in Figure 7 where the KBIs and specific corresponding residues are defined for the two binding modes.

Model 8 of part B of Table 1 is a highly unusual binding geometry when compared to the other 10 modes. The indanone ring in this model lies at the cavity bottom, there is a hydrogen bond between the carbonyl group of the indanone ring and the OH of Tyr 121, and the indanone ring is "parallel" to the indole side chain of Trp 84 at a distance of 3.58 Å. The intermolecular energy of this model is −44.27 kcal/mol, which makes it the tenth most stable complex of the 11 found. In this binding mode the dipoles of the enzyme and inhibitor are aligned in what appears to be a high-energy orientation. Nevertheless, this distinct, low-energy mode of binding does introduce some unusual design considerations when compared to the other identified binding models.

4. Binding Models of 2 to AChE. Analog **2** differs from **1** in two major ways. First, its more active (*S*) isomer is about 6× less active than the less active (*S*) isomer of **1**, see Table 1. Secondly, **2** is "shorter" than **1**, in that there is no methylene spacer between the indanone and piperidine rings. Receptor-independent 3D-QSAR studies[10–12] could not account for the loss in inhibition potency of **2**, and it was concluded that ligand–receptor modeling would be needed to account for the observed SAR of **2** relative to **1**. Thus, **2** has been considered in the receptor-dependent modeling reported here.

Thirteen docking models of **2** to E were found and are described in part C of Table 1. Seven of the models are for the *R* enantiomer, and six models for the *S* form. In all models the benzyl group lies at the bottom of the active-site gorge and the indanone ring lies near the entrance to this channel. In a similar manner to the binding of **1**, the piperidine ring of **2** lies at the narrowest part of aromatic gorge of the active site.
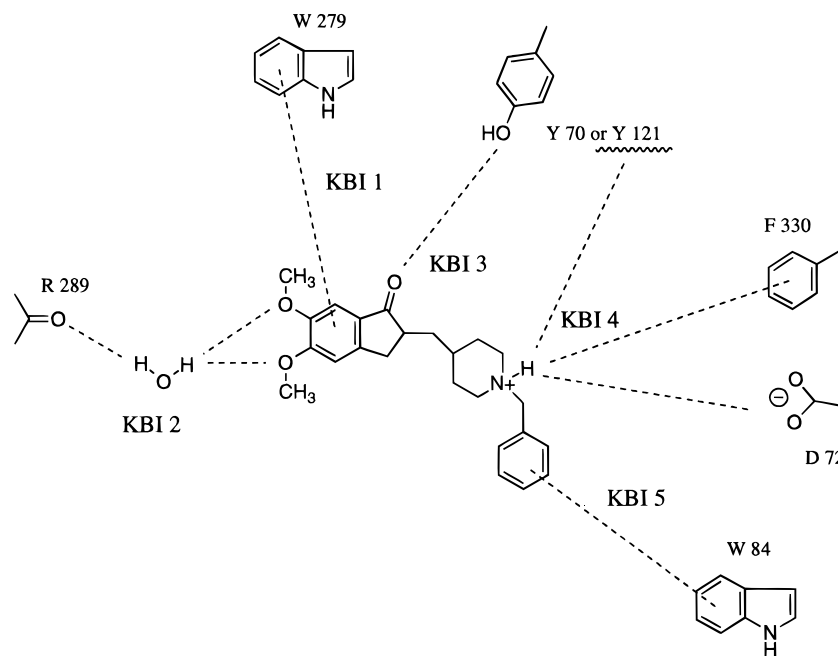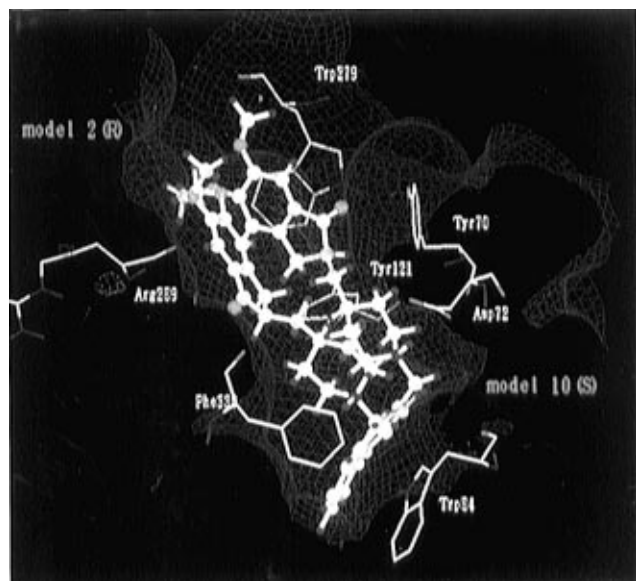
Figure 6. A drawing of the KBIs.

Figure 7. Superposition of the *R* and *S* isomers of **1** in their respective lowest-energy docking models to AChE with the KBI residues defined.

In six docking models the phenyl ring of the benzyl group is parallel to the indole side chain of Trp 84. No interaction is observed between indanone ring and Trp 279 in any of the models. The protonated piperidine NH forms a hydrogen bond with the hydroxy group of Tyr 121 in four models and with the carboxylate side chain of Asp 72 in two models. However, these two hydrogen bonds are simultaneously observed in only one model (10 of Table 2, part C).

Compound **2** can adopt a variety of low-energy orientations and positions in the active-site cavity of E. The short distance between the indanone ring and the benzylpiperidine for **2**, relative to **1**, prevents the interactions of the indanone ring with Trp 279, and the phenyl ring with Trp 84, to occur at the same time as is the case for **1**. Thus, while **2** adopts binding models which collectively are quite similar to those of **1**, the **2** binding modes do not realize as many of the KBIs as **1**. This leads to less stable ΔE_{total} values for **2**, relative to

1, which may be related to the higher K_i values for **2**. Of course, ΔE_{total} is a limited measure of the overall thermodynamics of ligand−receptor binding.

5. Docking Models of 3 to AChE. The racemic mixture of **3** has nearly the same activity as the *S* isomer of **1**. However, **3** is "longer" than **1**, having two methylene spacers between the indanone and piperidine rings; see Figure 1. Thus, the question arises regarding how this analog can be quite active while, in all likelihood, having a binding profile different from **1**. Compound **3** also could not be included in the construction of a receptor-independent 3D-QSAR.[10−12]

Twelve low-energy docking models of **3** to E were found and are reported in Table 1. In all of these models the benzyl group lies at the bottom of the active-site gorge and the indanone ring lies near the entrance to the gorge. Just like the other two inhibitors, the piperidine ring of **3** lies at the narrowest part of the gorge in all models.

In 10 of the docking models the phenyl group is parallel to the indole side chain of Trp 84 at an average distance of 3.49 Å. In four models the indanone ring is parallel to the indole side chain of Trp 279 at an average distance of 3.69 Å. In three models the protonated piperidine NH forms a hydrogen bond with the carboxyl group of Asp 72 at an average distance of 3.23 Å. The NH is pointed toward the center of the phenyl side chain of Phe 350 in three other models at an average distance of 4.67 Å. In four models the carbonyl group forms a hydrogen bond with the main chain of NH of Phe 288 at an average distance of 2.89 Å, and the carbonyl group forms a hydrogen bond with the hydroxy group in the side chain of Tyr 70 in four other models at an average distance of 2.96 Å.

Superimposing the binding models reveals that the enzyme−inhibitor complex structures involving **3** can be classified into two binding patterns which are shown in Figure 8. In one binding mode the indanone ring is parallel to the indole side chain of Trp 279, the carbonyl group forms a hydrogen bond with the hydroxy side chain of Tyr 70, and the protonated piperidine NH points toward the hydroxy side chain of Tyr 121 at an
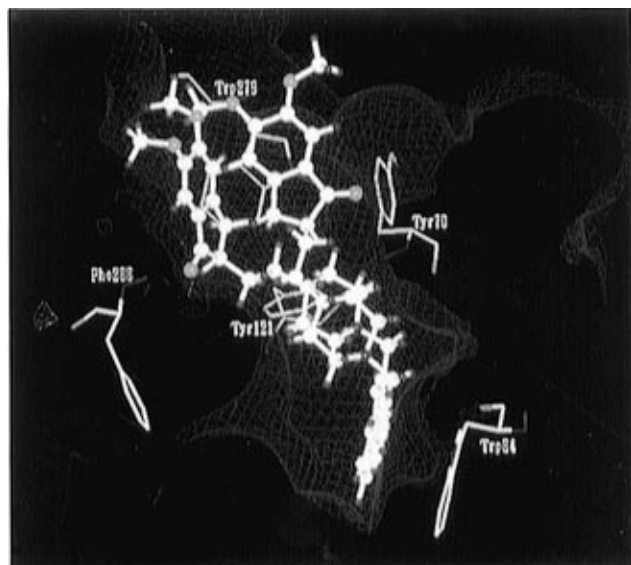
Figure 8. Superposition of the two classes of **3**−E binding models in the active-site cavity.

average interaction distance of 3.92 Å. This distance is too long for a hydrogen bond, but the geometry is conducive to the formation of a water bridge that has been observed between these groups.

In the other binding mode the indanone ring is perpendicular to the indole side chain in Trp 279, the carbonyl group forms a hydrogen bond with the NH main chain in Phe 288, and the protonated piperidine NH points toward the hydroxy side chain in Tyr 121. The hydrogen bond with Phe 288 represents a new subsite ligand−receptor interaction not seen in AChE−**1** binding models. The E_{total} values (see Table 1) of **3** are slightly lower (more stable) than those of **1**.

6. Comparison of Docking Models to Receptor-Independent 3D-QSARs. A receptor-independent 3D-QSAR was developed for a set of 15 compounds identical to **1** except for substitution onto the aromatic unit of the indanone ring,[10,11]

$$-\log \text{IC}_{50} = 2.21 C_4 - 6.65 U_T + 1.18 U_{T^2} - $$
$$162.99(\text{HOMO}) - 8.58(\text{HOMO})^2 - 757.2 \quad (3)$$

$$N = 15, \quad R = 0.94, \quad \text{SD} = 0.25, \quad F = 14.8,$$
$$U_T(\text{max}) = 2.8 \text{ Debye}, \quad \text{HOMO(max)} = -9.49 \text{ eV}$$

where IC_{50} is the applied concentration of inhibitor for 50% inhibition of AChE, C_4 is the HOMO out-of-plane π orbital coefficient of ring carbon four, U_T is the dipole moment of the substituted indanone ring, and HOMO, the highest occupied molecular orbital of the indanone ring.

A comparison of the descriptor terms in eq 3 to the KBIs of **1** suggest some possible associations between these two property sets. The U_T in eq 3 seems consistent with the dual formation of a hydrogen bond between the carbonyl group of the indanone ring and the hydroxyl of Tyr 121 (KBI 3a) and the oxygen in a methoxy group of the indanone ring forming a water bridge hydrogen bond with the carbonyl oxygen of Arg 289 (KBI2). C_4 and HOMO appear to be related to a partial π-stacking interaction between the indanone ring and the indole side chain of Trp 279 (KBI 1).

Substitution onto the benzyl group of **1** was also modeled and a 3D-QSAR constructed for 15 such

analogs[10,11]

$$-\log \text{IC}_{50} = -0.107 S_0 + 0.046(\text{IX}) - $$
$$0.151(\text{HOMO}) + 6.68 \quad (4)$$

$$N = 15, \quad R = 0.91, \quad \text{SD} = 0.60, \quad F = 16.7$$

where S_0 is the nonoverlap steric volume of the substituted benzyl of an analog, when aligned onto the unsubstituted benzyl analog, IX is the largest principal moment of inertia, and HOMO the highest occupied molecular orbital of the substituted benzyl group. Once again a comparison of 3D-QSAR descriptor terms to the preferred binding geometries of **1** gives insight as to why the QSAR descriptors are significant. As S_0 becomes larger, that is the substituents more bulky, inhibition potency is predicted by eq 4 to decrease. The low-energy docking models correspondingly suggest that substitution onto the benzyl ring cannot be sterically accommodated without a rearrangement in the docking alignment and, presumably, a loss in binding energy, see Figure 7. The IX descriptor in eq 4, when taken in conjunction with S_0, suggests that increasing the mass in the region of the benzyl group binding may increase inhibition potency. This relationship is not supported, or refuted, in the docking models of **1** to AChE. However, the change in entropy, due to conformational flexibility, upon binding should be less for higher mass substructures of a ligand and lead to higher inhibition activity, which is consistent with the positive regression coefficient of IX in eq 4. The HOMO term in eq 4 is consistent with optimizing the interaction of the benzyl ring with the indole ring of Trp 84 (KBI 5); again see Figure 7.

Molecular shape analysis, MSA, predicts that the "active" conformation of **1** (the receptor bound conformation) has the indanone ring "perpendicular" to the piperidine ring[11] as found in the X-ray structure of **1** and shown in Figure 9. This is clearly the same conformation found in all **1**−AChE binding modes.

On the other hand, MSA predicts[11] a conformation different from that seen in the X-ray structure of **1** to be the "active" (receptor-bound) conformation for the benzylpiperidine portion of the inhibitor. The MSA conformation can be characterized by the benzyl group "pointing" in the same direction in space as the carbonyl group on the indanone ring with respect to the inhibitor. The X-ray conformation of the benzylpiperidine moiety in **1** has the benzyl group extended away from the remainder of the molecule to give it a maximum length.

Conformational searching in the MSA study identified a third stable conformation of the benzylpiperidine moiety which is characterized by the benzyl group pointing in space in the "opposite" direction to the indanone carbonyl group. This third conformation is adopted in the low-energy docking models of **1** to AChE which is obvious from an inspection of Figure 7. Fortunately, the 3D-QSAR expressed by eq 4 is largely independent of total inhibitor conformation in terms of the values of S_0. Thus, the steric-restriction binding model embedded in eq 4, and supported by the docking studies, should be useful in inhibitor design even for the wrong benzylpiperidine binding conformation.

7. Docking Models for Acylated Enzyme (EA). Figure 10 shows a schematic representation of AChE inhibition and the formation of intermediates. Catalysis by AChE involves an active serine residue and the
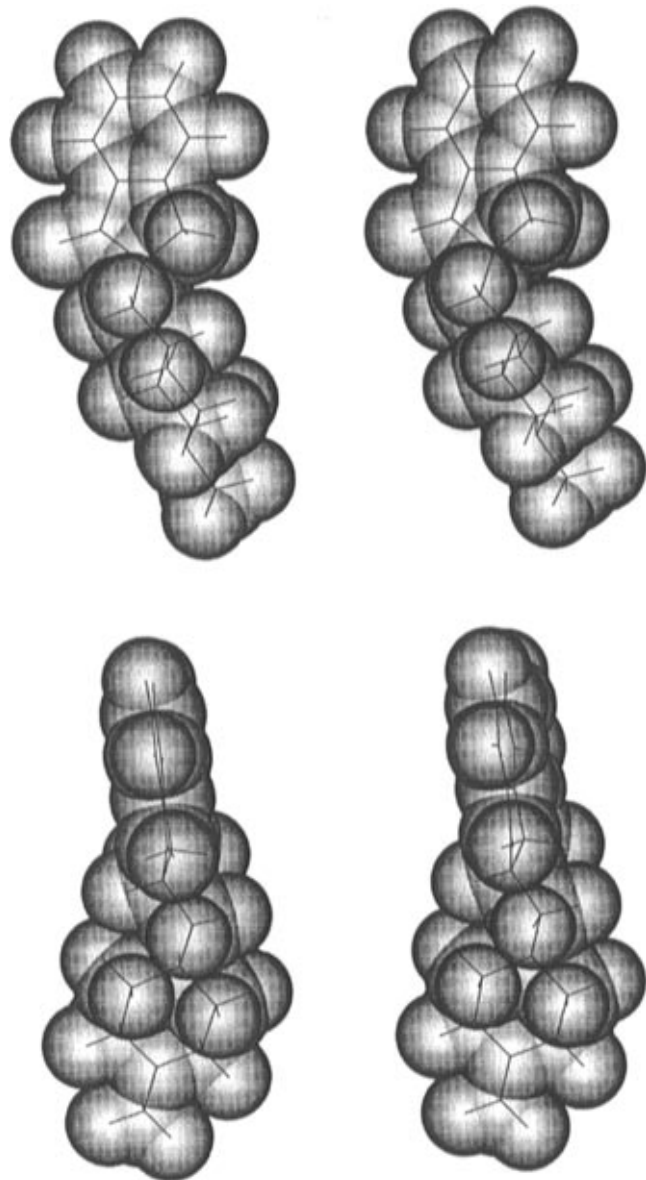
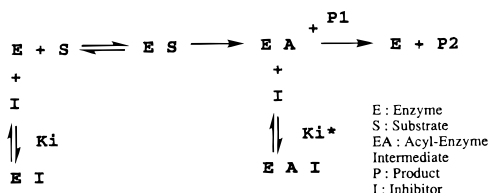**Figure 9.** The active (perpendicular) conformation of the indanone ring–piperidine ring moiety.

Figure 10. A schematic representation of the enzymatic reaction profile of AChE.

overall catalytic process proceeds in a three-step mechanism like transfer within a catalytic triad.[15] The activated serine residue enables a nucleophilic attack on ACh resulting in hydrolysis and acetate product being released. It is known that some reversible AChE inhibitors show a mixed type of inhibition by blocking the deacetylation process.[30–32] The acetyl group is introduced into the esteratic site in this catalytic process. Therefore, the acylated AChE enzyme, EA, can accept an external charged molecule at this vacant site to form an EA–inhibitor complex (EAI). As shown in Tables 1 and 2, **1** and related compounds, **2** and **3**, seem to bind to both the free enzyme and the acylated enzyme to block both Michaelis complex formation and the

Figure 11. Superposition of the optimized **1**–E binding complexes (red) on the **1**–EA binding complexes (green).

deacetylation process.[19] Thus, it is of interest to see if this dual inhibitory behavior can be explained/rationalized from the calculated binding models using the EA model of AChE described earlier.

The structures found from the docking studies with the free enzyme were used as the initial geometries for **1** and its analogs with EA in the docking studies, see Table 2, part A. Superposition of the optimized **1**–EA binding complexes on the **1**–E complexes, shown in Figure 11, indicates that each of the 111 respective binding models of EA and E are quite similar, except for model 5. The inhibitor in model 5 relocates in the EA binding cavity, and KBI 1 is lost, KBI 4 changes, and the total binding energy is lower (more stable) relative to E. Overall, **1** appears to interact with the EA in much the same conformation and intermolecular binding modes as with E. In the **1**–EA binding complexes the indanone ring is parallel to the indole side chain of Trp 279 at an average distance of 3.84 Å. A methoxy group is positioned near the main chain carbonyl of Arg 289, and its oxygen could interact with the enzyme through a water bridge. The carbonyl group of **1** forms a hydrogen bond with the hydroxy side chain of Tyr 121 in two binding models (*R* form) and with the hydroxy side chain of Tyr 70 in one model (*S* form). The protonated piperidine NH points toward the carboxlate side chain of Asp 72 in all three of these models even though a hydrogen bond does not form. The distance between the nitrogen and the oxygen varies from 3.11 to 3.90 Å in these binding models. The phenyl ring is parallel to the indole side of Trp 84 at an average distance of 4.14 Å. In Table 2, part A, the last column labeled "rms" lists the root-mean-square displacement of the **1** atoms in each EA binding model as compared to the corresponding binding model for E.

Compounds **2** and **3** each mimic their respective binding modes to E when docked to EA. The details of each of the binding models for these two inhibitors are reported in parts B and C of Table 2.

Overall, the ΔE_{intra}, E_{inter}, and E_{total} are quite close to one another for each respective inhibitor to E and EA. This suggests these inhibitors should be about equally

potent for both the free and acylated forms of AChE. A comparison of the binding energies of **1** as a function of both isomer form and E and EA indicates that the *R* isomers have somewhat lower E_{total} values than the *S* isomers for E which is consistent with the observed K_i (Table 1, part B). However, model 7, an *S* isomer binding model is about equally stable to the lowest-energy model of the *R* isomer (model 2) for **1** bound to EA.

Discussion

The dipole moments of the static binding conformations of ACh and inhibitors **1**, **2**, and **3** to E have been calculated. The estimated large dipole of AChE aligned along the axis of the gorge leading to the active site, the large dipole of ACh, the even larger dipoles of **1** and its active inhibitor analogs, and the calculated general modes of ACh and inhibitor binding to AChE suggest that the gross features of ligand−receptor binding for AChE can be characterized by a narrow cylindrical ligand, possessing a large dipole running the length of the cylinder which "slides" down the gorge of AChE such that its dipole is in a complementary direction of AChE. However, once these general requirements of ligand−receptor binding are met, the behavior of ligand−AChE binding become complex and quite subtle according to our binding simulations.

While other AChE−ligand docking studies have been performed on the compound **1** types of inhibitors,[17,18] the studies reported here are the first for which ligand and receptor flexibility has been allowed, and extensive intraligand and ligand−receptor energetics used in defining the preferred binding modes. Perhaps it is these added features to the binding simulations which have allowed the probing of ligand−receptor behavior that does not seem to have surfaced in previous studies.

One of the subtle findings is that the lowest-energy docking model for ACh to AChE (see Table 1, part A) has the carboxyl oxygen of ACh in close contact with Gly 118 and 119 and the choline moiety "binding" to aromatic residues in the gorge. This model is in contrast to the proposed ACh binding mode where the cholien unit makes a close contact with the indole ring of Trp 84[27] and is about 3 kcal/mol higher in energy in our binding simulations than the lowest-energy model of part A of Table 1.

Ligand−AChE binding behavior becomes even more complex for **1** and its analogs. In a previous study[17] **1** was calculated to bind to AChE such that there are interactions between the indanone ring and Trp 279 (KBI 1) as well as the carbonyl oxygen of the indanone ring and the hydroxyl group of Tyr 121 (KBI 3a). The benzyl group was observed to interact with Trp 84 (KBI 5). Our docking simulations indicate that this mode of binding is a low-energy docking model (see models 1, 5, and 6 of Table 1, part B). However, it is not the only binding mode, nor is it the lowest-energy binding mode. Other significant ligand−receptor interaction sites, KBIs, have been identified, and combinations of these KBIs give rise to many low-energy binding models as reported in part B to Table 1.

Whether such a large number of binding modes of **1** to AChE actually occurs or this binding multiplicity is a product of an incomplete thermodynamic analysis coupled with the use of a limited force field cannot be acertained. However, it does appear that the **1**−AChE complex can exhibit an independent subsite binding behavior. That is, there can be the same KBIs, except for one ligand subsite where there are two, or more, distinct KBI binding modes. The single change/difference at one binding subsite does not influence the binding at other subsites. Binding models 3 and 5 in Table 1, part B, demonstrate subsite binding independence. A change in KBI 3 does not alter the other common KBIs of these two binding modes. Of course, there are other pairs of **1**−AChE binding modes which are very different from one another and the independent subsite binding model is not valid; see, for example, models 10 and 11 of part B of Table 1.

The overall characteristic binding behavior of both **2** and **3** is the same as **1**. However, it is worth mentioning that the near-equal activity of **3** to **1** could not be established by receptor-independent MSA studies.[10,11] The inability to include analogs with two, or more, methylene spacers between the indanone and piperidine rings in an MSA 3D-QSAR precluded making predictions on inhibition potency. It was *postulated* that these "larger" analogs were active because they could fit into AChE. The docking simulations reported here for **3** establishes not only that this analog fits into the active site gorge of AChE but that is computed binding energy is about the same as **1**.

The lack of activity of **2**, relative to **1**, could not be accounted for in the MSA 3D-QSAR studies.[10,11] Docking simulations indicate that this "short" analog cannot realize enough KBIs to have a binding energy on par with **1**. While this binding behavior was speculated in the receptor-independent modeling studies, the docking simulations provide evidence for this assertion.

Perhaps even more gratifying is that the docking simulation energetics are consistent with the observed K_i values for **1** and its two analogs. The binding models provide insight into the origin of the high inhibition potency of each of the two **1** isomers. The docking energetics also suggest, in agreement with the observed K_i, that the *R* isomer (model 2 of part B of Table 1) should be a more potent inhibitor than the *S* isomer (model 10).

Docking simulations with an acylated AChE model also provide a basis for explaining the observed dual inhibitory activity of **1**, and many of its analogs, to both the free and acylated forms of the enzyme. Overall, the calculated modes of binding of **1**, and its two analogs, to EA are both energetically and geometrically very similar, respectively, to E.

Comparisons of the docking geometries to the corresponding MSA 3D-QSARs provide insights greater than that of the "sum" of the two CAMD models (3D-QSAR and binding modes). An inspection of the type of binding interaction to the corresponding QSAR descriptor(s) suggests a straightforward interpretation of why the descriptor is significant, and both models then support one another. Moreover, the quantitative nature of the descriptors in the QSARs provide guidelines as to how to modify the inhibitor in order to optimize the binding interaction. For example, the C_4 and HOMO descriptor terms in eq 3 suggest criteria needed to maximize inhibition activity as a function of substitution onto the indanone ring. This presumably corresponds to optimizing the "aromatic" interaction of the indanone ring of the inhibitor with the indole side chain of Trp 279. In composite, combining the findings from the MSA 3D-QSAR studies[10,11] with the docking simulation

models reported here permits a detailed understanding of the observed structure−activity profile of well over 100 compounds "related" to **1**.

Still, the SARs of the **1** classes of AChE inhibitors contain some unusual behavior. The trans decalin analog (see Figure 1) was predicted to be quite active ($IC_{50} \sim 10^{-9}$) based upon MSA 3D-QSAR analysis.[10,11] This compound was found to be relatively inactive ($IC_{50} \sim 10^{-6}$). The source of the inactivity was assumed to be due to unfavorable ligand−receptor interactions. However, our docking analysis indicates that the trans decalin analog can bind to AChE in most of the binding modes given in Table 1, part B, and the trans decalin analog has a total binding energy, $E_{total} = -51.9$ kcal/mol for a binding model very similar to model 1 in part B of Table 1. Thus, we are at a loss to explain the low inhibitory activity of this compound.

Recent hydrated molecular dynamics simulations of isolated AChE (no inhibitor or substrate present) have identified a "back door" opening to the active site located along the active-site gorge.[33] Our water-independent simulation studies of AChE with bound ACh, and some inhibitors, does not indicate that a backdoor can form a large enough opening for a long enough time period to permit the entry, or exit, of ligands and/or products to the active site. However, it is possible that waters may facilitate the relaxation and dilation of such an opening.

We also realize that our docking simulations, in addition to not including solvation, also neglect entropy and the energetics of AChE without a ligand. It is also quite likely that any force field used will have shortcomings in accurately estimating binding thermodynamics, and some type of calibration of the force field will be needed to customize it to the specific ligand−receptor system. Our hope is to tackle all of these difficulties by employing a new method, called free-energy force field QSAR analysis,[34] which customizes force fields for specific chemical systems.

References

(1) Homma, A.; Hasegawa, K.; Nishimura, T.; Kameyama, M.; Hariguchi, S.; Imai, Y. Clinical Efficacy Of E-2020 in Treatment of Patients with Probable Alzheimer's Disease: Part 2. Double Blind Placebo Controlled Study. In *The Proceedings of 6th Congress of the International Psychogerica Association*, 1993.

(2) Yamanishi, Y.; Ogura, H.; Kosasa, K.; Araki, S.; Sawa, Y.; Yamatsu, K. Inhibitory Action of E2020, A Novel Acetylcholinesterase Inhibitor, on Cholinesterase: Comparison with Other Inhibitors. In *Basic, Clinical, and Therapeutic Aspects of Alzheimer's and Parkinson's Diseases, Volume 2*; Plenum Press: New York, 1990; p 409.

(3) Bartus, R. T.; Dean, R. L., III; Beer, B.; Lippa, A. S. The Cholinergic Hypothesis of Geriatric Memory Dysfunction. *Science* **1982**, *217*, 408.

(4) Sims, N. R.; Bowen, D. M.; Allen, S. J.; Smith, C. C. T.; Neary, D.; Thomas, D. J.; Davison, A. N. Presynaptic Cholinergic Dysfunction in Patients. *J. Neurochem.* **1983**, *40*, 503.

(5) Gottfries, C. G. Pharmacological Treatment Strategies in Alzheimer Type Dementia. *Psychopharmacology* **1985**, *86*, 245.

(6) Perry, E. K. The Cholinergic Hypothesis-Ten Years on. *Br. Med. Bull.* **1986**, *42*, 63.

(7) Summers, W. K.; Koehler, A. L.; Marsh, A. M.; Tachiki, K.; Kling, A. Long-Term Hepatotoxicity of Tacrine. *Lancet* **1989**, *33*, 729.

(8) Sugimoto, H.; Tsuchiya, Y.; Sugumi, H.; Higurashi, K.; Karibe, N.; Iimura, Y.; Sasaki, A.; Kawakami, Y.; Nakamura, T.; Araki, S.; Yamanishi, Y. Novel Piperidine Derivatives. Synthesis and Anti-Acetylcholinesterase Activity Of 1-Benzyl-4-[2-(N-benzoylamino)ethyl]piperidine Derivatives. *J. Med. Chem.* **1990**, *33*, 1880.

(9) Kawakami, Y.; Inoue, A.; Kawai, T.; Wakita, M.; Sugimoto, H.; Hopfinger, A. J. The Rationale for E2020 as a Potent Acetylcholinesterase Inhibitor. *BioOrg. Med. Chem.*, in press.

(10) Cardozo, M. G.; Imura, Y.; Sugiomoto, H.; Yamanishi, Y.; Hopfinger, A. J. QSAR Analyses of the Substituted Indanone and Benzylpiperidine Rings of a Series of Indanone-Benzylpiperidine Inhibitors of Acetylcholinesterase. *J. Med. Chem.* **1992**, *35*, 584.

(11) Cardozo, M. G.; Kawai, T.; Iimura, Y.; Sugimoto, H.; Yamanishi, Y.; Hopfinger, A. J. Conformational Analyses and Molecular-Shape Comparisons of a Series of Indanone-Benzylpiperidine Inhibitors of Acetylcholinesterase. *J. Med. Chem.* **1992**, *35*, 590.

(12) Kawakami, Y.; Kawai, T.; Inoue, A.; Iimura, Y.; Sugimoto, H.; Yoshida, Y.; Sato, T. E2020: The Rational Design of a Potent Acetylcholinesterase Inhibitor. In *The Proceedings of 14th Symposium on Medicinal Chemistry (Japan)*, **1993**, p 19.

(13) Ishihara, Y.; Hirai, K.; Miyamoto, M.; Goto, G. Central Cholinergic Agents. 6. Synthesis and Evaluation of 3-[1-(Phenylmethyl)-4-piperidinyl]-1-(2,3,4,5-tetrahydro-1H-1-benzazepin-8-yl)-1-propanones and Their Analogs as Central Selective Acetylcholinesterase. *J. Med. Chem.* **1993**, *37*, 2292.

(14) Villalobos, A.; Blake, J. F.; Biggers, C. K.; Butler, T. W.; Chapin, D. S.; Chen, Y. L.; Ives, J. L.; Jones, S. B.; Liston, D. R., Nage, A. A.; Nason, D. M.; Nielsen, J. A.; Shalaby, I. A.; White, W. F. Novel Benzisoxazole Derivatives as Potent and Selective Inhibitors of Acetylcholinesterase. *J. Med. Chem.* **1994**, *37*, 2721.

(15) Tong, W.; Collantes, E. R.; Yu, C.; Welsh, W. J. A Comparative Molecular Field Analysis Study of N-Benzylpiperidines as Acetylcholinesterase Inhibitors. *J. Med. Chem.* **1996**, *39*, 380.

(16) Sussman, J. L.; Harel, M.; Frolow, F.; Offner, C.; Goldman, A.; Toker, L.; Siman, I. Atomic Structure of Acetylcholinesterase from Torpedo californica: A Prototypic Acetylcholine-Binding Protein. *Science* **1991**, *253*, 872.

(17) Yamamoto, Y.; Ishihara, Y.; Kuntz, I. D. Docking Analysis of a Series of Benzylamino Acetylcholinesterase Inhibitors with a Phthalimide, Benzoyl, or Indanone Moiety. *J. Med. Chem.* **1994**, *37*, 3141.

(18) Yuan-Ping, P.; Alan, P. K. Prediction of the Binding Site of 1-benzyl-4-[(5,6-dimethoxy-1-indanon-2-yl)methyl]piperidine in acetylcholinesterase by Docking Studies with the SYSDOC Program. *J. Comput. Aided Mol. Des.* **1994**, *8*, 683.

(19) Nochi, S.; Asakawa, N.; Sato, T. Kinetic Study on the Inhibition of Acetylcholinesterase by 1-Benzyl-4-[(5,6-dimethoxy-1-indanon)-2-yl]methylpiperidine Hydrochloride (E2020). *Biol. Pharm. Bull.* **1995**, *18*, 1145.

(20) (a) Tomioka, N.; Itai, A. GREEN: A Program Package for Docking Studies in Rational Drug Design. *J. Comput.-Aided Mol. Des.* **1994**, *8*, 347. (b) GREEN V4.0, PDBFIL. Distributed by the Institute of Medicinal Melecular Design, 5-24-5, Hongo, Bunkyo-ku, Tokyo 113, Japan (1995).

(21) Weiner, S. J.; Kollman, P. A. An All Atom Force Field for Simulations of Proteins and Nucleic Acids. *J. Comput. Chem.* **1986**, *7*, 230.

(22) Dewer, M. J. S.; Thiel, W. Ground States of Molecules. 38. The MNDO Method. Approximations and Parameters. *J. Am. Chem. Soc.* **1977**, *99*, 4899.

(23) Insight II/DelPhi, Release 95.0. Distributed by the Molecular Simulations Inc., 9685 Scranton Rd., San Diego, CA 92121-3752, 1995.

(24) CAVHET is the original program developed by A. Inoue. Eisai Tsukuba Research Laboratories, 5-1-3, Tokodai, Tsukuba, Ibaraki 300-26, Japan, 1995.

(25) Nelder, J. A.; Mead, R. A simplex method for function minimization. *Comput. J.* **1965**, *7*, 308.

(26) Hopfinger, A. J. *Conformational Properties of Macromolecules*; Academic Press: New York, 1973.

(27) Harel, M.; Shalk, I.; Ehret-Sabatier, L.; Bouet, F.; Goeldner, M.; Hirth, C.; Axelsen, P. H.; Silman, I.; Sussman, J. L. Quaternary Ligand Binding to Aromatic Residues in the Active-Site Gorge of Acetylcholinesterase. *Proc. Natl. Acad. Sci. U.S.A.* **1993**, *90*, 9031.

(28) Ripoll, D. R.; Faermam, C. H.; Axelsen, P. H.; Silman, I.; Sussman, J. L. An Electrostatic Mechanism for Substrate Guidance Down the Aromatic Gorge of Acetylcholinesterase. *Proc. Natl. Acad. Sci. U.S.A.* **1993**, *90*, 5128.

(29) Raymond, C. T.; Thanh, N. T.; McCammon, J. A. Acetylcholinesterase: Electrostatic Steering Increases the Rate of Ligand Binding. *Biochemistry* **1993**, *32*, 401.

(30) Krupka, R. M.; Laidler, K. J. Molecular Mechanisms for Hydrolytic Enzyme Action. I. Apparent Non-competitive Inhibition, with Special Reference to Acetylcholinesterase. *J. Am. Chem. Soc.* **1961**, *83*, 1445.

(31) Krupka, R. M.; Laidler, K. J. Molecular Mechanisms for Hydrolytic Enzyme Action. III. A General Mechanism for the Inhibition of Acetylcholinesterase. *J. Am. Chem. Soc.* **1961**, *83*, 1454.

(32) Krupka, R. M. Acetylcholinesterase: Structural Requirements for Blocking Deacetylation. *Biochemistry* **1965**, *4*, 429.

(33) Gilson, M. K.; Strastsma, T.; McCammon, J. A. Open "Back Door" in a Molecular Dynamics Simulation of Acetylcholinesterase. *Science* **1994**, *263*, 1276.

(34) Hopfinger, A. J.; Tokarski, J. Private communication.